Optica Applicata, Vol. XXXVI, No. 1, 2006

Laser aerosol time-of-flight mass spectrometry analysis of individual aerosol particles from photooxidation of toluene

MING-QIANG HUANG, ZHEN-YA WANG, LI-QING HAO, LIU-ZHU ZHOU, XUE-JUN GU, LI FANG, WEI-JUN ZHANG

Laboratory of Environment Spectroscopy, Anhui Institute of Optics and Fine Mechanics, Chinese Academy of Sciences, Hefei 230031, China

A laser aerosol time-of-flight mass spectrometry (ATOFMS) that can be used for real-time measurement of the size and composition of individual aerosol particles has been designed and manufactured in our laboratory. Particles are introduced into the instrument through a particle beam interface, sized by measuring the delay time between two scattering lasers, and compositionally analyzed using a laser desorption/ionization linear-time-of-flight mass spectrometry. Secondary organic aerosol particles from the photooxidation of toluene in the CH_3ONO/NO/air mixture were generated in a home-made smog chamber and measured using it. Experimental results showed that the individual aerosol particles from photooxidation of toluene can be measured in real-time by this instrument. This unique capability is impossible in off-line methods such as chromatography and chemical method.

Keywords: secondary organic aerosol (SOA), laser desorption/ionization, laser aerosol time-of-flight mass spectrometer (ATOFMS).

1. Introduction

Aerosol formed in the atmosphere through condensation of low vapor pressure organic oxidation products is referred to as secondary organic aerosol (SOA) [1]. Interest in SOA formation in the atmosphere has been renewed because of its possible impacts on the radiative balance associated with climate change, visibility degradation, and public health. Benzene, toluene, ethylbenzene, and xylene are aromatic hydrocarbons, and toluene is the most abundant aromatic hydrocarbon among them [2]. Aromatic hydrocarbons play a dominant role in the formation process of secondary organic aerosols [3]. In the last 10 years, the studies on formation mechanism [2, 4–9] and detection methods [2, 5, 10–12] of aromatic SOA are of particular interest. A routine way to measure the size of SOA particles is using scanning electrical mobility spectrometer (SEMS) and to count transmitted particles a condensation nuclei counter

(CNC) is used [8]. Chemical composition was analysed by gas chromatograph/mass spectrometer [5, 8]. The particles are collected using filters and samples are prepared by the way of chemical extracts. More molecular compositions of SOA could also be analyzed with a positive chemical ionization (CI) gas chromatography ion trap mass spectroscopy (GC-TIMS) [2, 10–12]. By the way, the Fourier transform infrared spectroscope (FTIR) is used to obtain additional functional group information for SOA products. However, the measurement of particle size and chemical composition was performed separately and only a statistical result about the particles was obtained. The information involved in the individual particle was ignored. Furthermore, there are some disadvantages in GC/MS and CI-GC-TIMS systems, for example, possible secondary chemical reactions or loss of semivolatile compounds associated with traditional aerosol sampling onto a filter or impactor plate, or with multi-step chemical treatments.

Over the past decade, a number of real-time single particle mass spectrometry (RTSPMS) techniques have been developed, offering new opportunities for studying aerosol particulate matters [13]. Among RTSPMS laser aerosol time-of-flight mass spectrometry (ATOFMS) can be used to determine in real-time both the size and chemical composition of individual particle [14, 15]. The ATOFMS can overcome those disadvantages met in GC/MS and CI-GC-TIMS systems. It analyses composition nearly immediately and in real-time, and the size and chemical composition of individual particle is measured simultaneously [16–18]. The size distribution has also been obtained. From the composition of a large number of individual particles, the composition of the SOA particle can be determined statistically. So, the present study represents a comprehensive effort to use home-made ATOFMS to analysis of individual aerosol particles from photooxidation of toluene.

2. Experiment

2.1. Laser aerosol time-of-flight mass spectrometry (ATOFMS)

Figure 1 shows a schematic diagram of the experimental configuration. The overall system includes three distinct regions: i) an aerosol introduction interface, which includes three adjustable stages of differential pumping; ii) a light scattering region for particle detection and velocity/size determination; and iii) a linear-time-of-flight mass spectrometry for single particle composition analysis [19, 20].

2.1.1. Aerosol introduction interface

The aerosol introduction interface consists of a nozzle followed by a series of three differentially pumped regions separated by skimmers. The three interface regions operate at a pressure of 2.0, 4.5×10^{-1}, 7.5×10^{-5} torr, achieved using 3 mechanical pumps and 1 molecule pump with speeds of 8 and 150 L/s. The ultimate pressure in the detector region of the mass spectrometry is 7.5×10^{-5} torr. The particles first enter

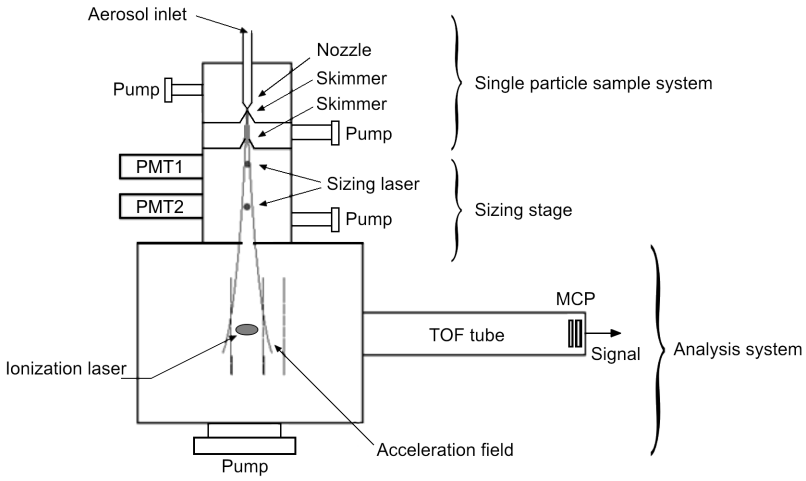

Fig. 1. Schematic showing the laser aerosol time-of-flight laser mass spectrum.

the inlet nozzle at atmospheric pressure (760 torr) and exit at a pressure of 2 torr. This pressure differential causes the gas to undergo a supersonic expansion, during which small particles are accelerated to a higher terminal velocity than large particles. The aerosol undergoes expansion through the nozzle to produce particles with velocities ranging between 100 and 400 m/s which travel through successive skimmers to produce a collimated aerosol beam.

2.1.2. Particle sizing region

We use the technique of determining the aerodynamic diameter developed by Prather and co-workers. This technique, uses light scattering from two lasers to determine aerodynamic diameter to within 1% [17]. The principle is shown in Fig. 2. Upon exiting the interface region, the particles travel in the form of a narrow beam into the light scattering region. Each particle first encounters light from a red continuous-wave, diode-pumped laser operating at 650 nm focused to a 0.1 mm spot size. The scattered light from the particle is collected by a lens and fiber-optic system and detected by a photomultiplier detector (PMT1, Fig. 1). The particle travels a set distance (70 mm) further where it encounters a second laser, a focused 50 mW red continuous-wave, diode-pumped laser operating at 650 nm focused down to 0.1 mm. Scattered light from this laser is collected by a lens and fiber-optic system and transferred to another photomultiplier detector (PMT2, Fig. 1). In the ATOFMS system, the two scattering lasers are oriented at right angles to one another to ensure that the detected particle is travelling along the centered path necessary to reach the desorption/ionization region of the linear-time-of-flight mass spectrometry. Both light scattering signals are passed on to an external electronic timing circuit used to track the particles through the system. From the external electronic timing circuit, we can measure the transit time and

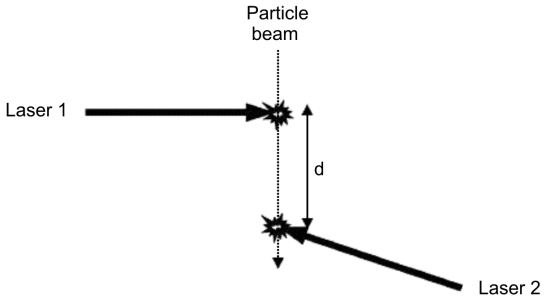

Fig. 2. Principle of determining the particle's aerodynamic diameter.

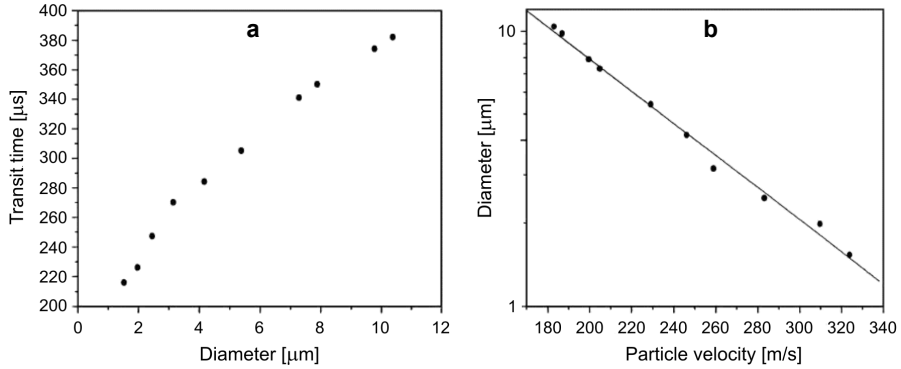

Fig. 3. Transit time *vs*. aerodynamic diameter of individual DOP particles (**a**), aerodynamic diameter *vs*. velocity of individual DOP particles (**b**).

the velocity of the particle. The velocity of the particle is directly related, and upon performing appropriate calibration studies, this relationship will be used for determination of individual particle size. Thus, the light scattering region serves two purposes: determination of particle size/velocity and detection of the incoming particle and its associated velocity, allowing synchronization of the firing pulse of the desorption/ionization lasers with the arrival of the particle in the source region of the mass spectrometry.

The correlation between transit time and aerodynamic particle size can be established experimentally using particle of known size and composition. In our laboratory, calibration of the particle-sizing region was accomplished by a commercially available vibrating orifice aerosol generator (TSI, Inc., Model 3450), ranging in size from 1.53 to 10.4 μm in diameter. This particular aerosol generation system was chosen because of its ability to provide monodisperse, micrometer-sized particles, all of known size (within 1%) and chemical composition. We use TSI 3450 to generate 10 different diameters of diocyl phthalate (DOP) particle, ranging from 1.53 to

10.4 μm.We measured the transit time, as shown in Fig. 3, and gained the relationship of transit time as a function of aerodynamic particle size, or aerodynamic particle size as a function of velocity of the DOP particle in the 1.53–10.4 μm size range [19]. These data can be fit well by the following equation:

$$D_p = 117.49 \times 10^{-0.0059V}$$

where D_p is the diameter of the particle, and V is the velocity of the particle.

2.1.3. Linear time-of-flight mass spectrometry

After exiting the light scattering region, the particle enters the source region of a linear time-of-flight mass spectrometry. The electronic timing circuit, based on the measured time delay between the two red continuous-wave, diode-pumped laser scatter pulses and the relative distances between them, triggers a pulsed Nd:YAG laser operating at the fourth harmonic (266 nm), and the laser power is 10^8/cm^2. Upon absorption of the laser pulses, the particle is heated in a rapid fashion, desorbing and ionizing individual molecules from the particle. The resulting ions are accelerated by positive (or negative) electric field created by a series of source plates at different voltages. Ions with a lower mass-to-charge ratio (m/z) are accelerated to higher velocities than ions with a higher ratio. Then, ions enter the flight tube (the inner diameter is 100 mm, and the length is 1000 mm), and the ion signal is detected by a dual microchannel plate detector fixed at the end of the flight tube and sent to a pre-amplifier, then the amplified ion signal is recorded by a transient recorded interfaced to a personal computer.

2.2. Smog chamber experiment

Secondary organic aerosol from the photooxidation of toluene in the CH_3ONO/NO/air mixture was generated in 22.4 L smog chamber [21]. Prior to starting the experiment, the chamber was continuously flushed with purified laboratory air for 20 minutes, and evacuated to a vacuum of 10^{-1} Pa by a mechanical pump. The purified air was processed in three consecutive packed-bed scrubbers containing, in order, activated charcoal, silica gel and a Balston DFU® filter (Grade BX), respectively, to remove the trace of hydrocarbon compounds, moisture and particles. Toluene was sampled by a microliter injector and injected directly into the chamber. The NO and methyl nitrate were expanded into the evacuated manifold to the desired pressure through Teflon lines, and introduced into the smog chamber by a steam of purified air. The whole system was completely shrouded from sunlight with a black polyethylene tarpaulin. After injection of the reactant gases into the smog chamber, the purified air was introduced into it again until the pressure within it reached 10^5 Pa. Then, four blacklamps were turned on to begin the photooxidation experiment for 90 minutes. At the end of reaction, the SOAs produced by the photooxidation were analyzed continuously using the ATOFMS connected directly to the chamber with a Teflon line.

3. Result and discussion

According to the design principles of the measuring system of particle diameter, timing circuit, and laser desorption/ionization setup of ATOFMS, its time of flight mass spectroscopy is only obtained from those particles of secondary organic aerosol whose diameter has been measured. The diameter of individual particle, number distribution of SOA particle diameter, and molecular composition of SOA particle could be measured using our ATOFMS.

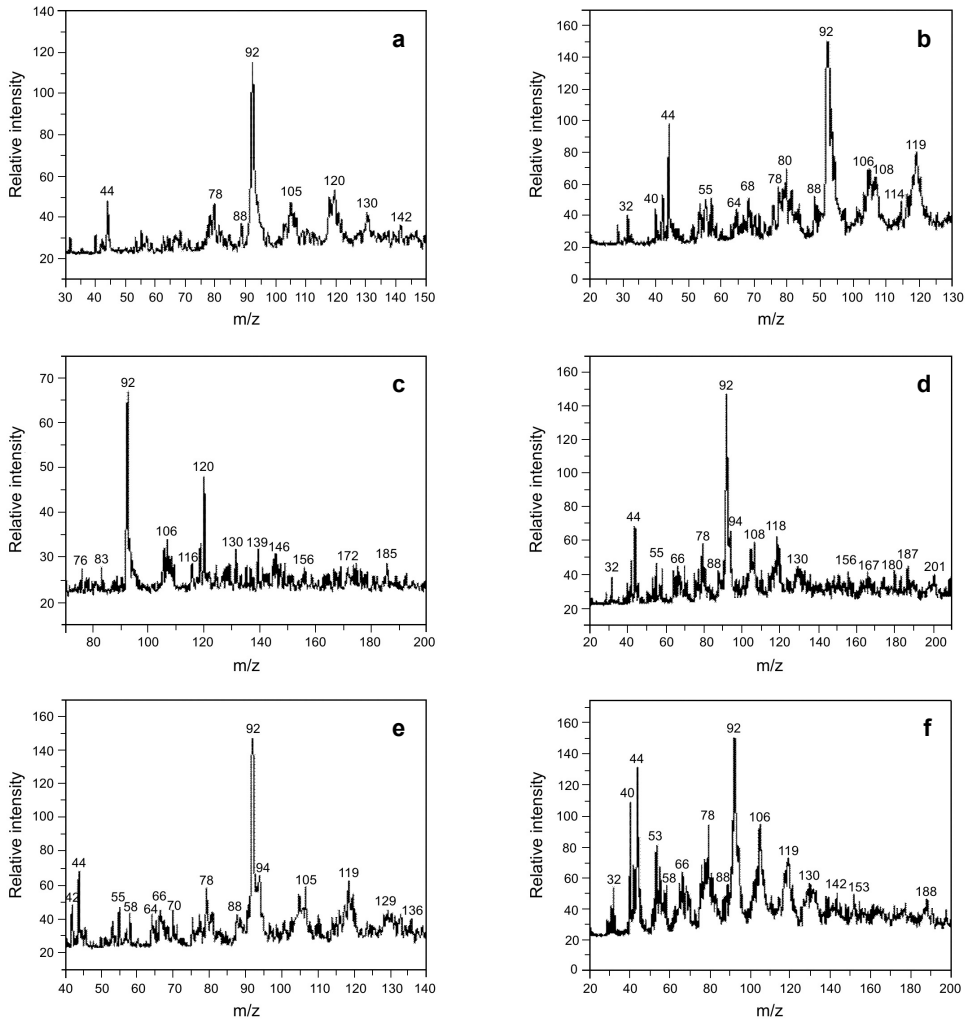

Fig. 4. Positive ion mass spectra of individual particles: aerosol diameter 1.564 μm (**a**), aerosol diameter 0.724 μm (**b**), aerosol diameter 2.142 μm (**c**), aerosol diameter 1.986 μm (**d**), aerosol diameter 1.848 μm (**e**), aerosol diameter 1.684 μm (**f**).

3.1. Size and composition of individual particle

The chemical composition and size of individual SOA particles produced from the photooxidation of toluene are shown in Fig. 4. It is said that each piece of mass spectrum corresponds to an aerosol particle, and the diameter and chemical composition might be different from each other.

3.2. Size distribution

The number distribution of SOA particles, produced from photooxidation of toluene, as a function of particle size is shown in Fig. 5. In these SOA particles, the smallest

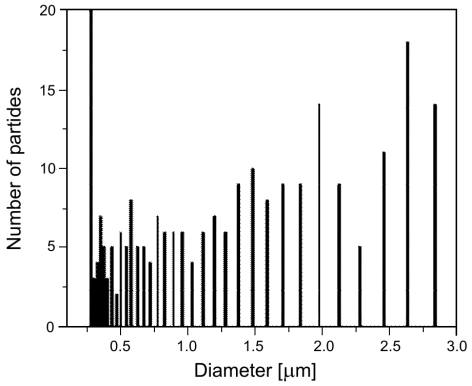

Fig. 5. Diameter distribution of SOA particles detected by ATOFMS.

and the largest diameters of the particle are about 0.1 and 2.7 μm, respectively, most of them being about 0.1–2.5 μm.

3.3 Chemical composition of SOA

When the diameter and chemical composition of the SOA particle are detected using ATOFMS, the allowable error of the ratio of mass to charge (m/z) is about ±0.5 [22]. From Fig. 4 and a large number of other mass spectra, the chemical composition of SOA particle might be known statistically. Enclosed here are some ratios of mass to charge from a large number of mass spectra: 32, 40, 42, 44, 48, 52, 54, 58, 64, 66, 68, 70, 78, 88, 92, 94, 106, 108, 114, 119, 130, 142, 153, 180, 185, 188 and 202. Each ratio of mass to charge corresponds to a different compound molecule. According to the references and possible reaction pathways of toluene photooxidation reaction, we assigned m/z = 40, 48, 52, 54 and 66 as polymer of C, or hydrocarbons of C and H, C_3H_4, C_4, C_4H_4, C_4H_6 and C_5H_6; m/z = 42 as ketene C_2H_2O [23]; m/z = 44 as acetaldehyde C_2H_4O [2]; m/z = 68 as furan C_4H_4O [2, 23]; m/z = 78 as benzene C_6H_6; m/z = 88 as 2-hydroxy-1,3-propandial or 2-oxopropanic acid $C_3H_4O_3$ [2]. The strongest signal in mass spectrum is toluene ($C_6H_5CH_3$, m/z = 92); m/z = 94 as phenol [2], while

m/z = 106 as benzaldehyde C_7H_6O [2, 5]; m/z = 108 as benzyl alcohol or *o*-cresolm (*m*-, *p*-isomers) C_7H_8O [2,5]; m/z = 114 as 4-oxo-2-pentenoic acid $C_5H_6O_3$ [2]; m/z = 130 as 3-hydroxy-2,4-dioxo-pentanal $C_5H_6O_4$ [2]; m/z = 142 as 4,5-dioxo-2--hexenoic acid $C_6H_6O_4$ [2]; m/z = 153 as 4-methyl-2-nitrophenol $C_7H_7NO_3$ [2] while 32, 119, 180, 185, 188 and 201 respresent some unidentified compounds.

From our experimental results and discussion mentioned above, it is shown that in these molecules and radicals detected using ATOFMS, some of them are produced from H-atom abstraction from the methyl group of toluene and some from $OH^{\cdot}$ addition to the benzene ring in the toluene reaction. The chemical compositions identified in the SOA particles can also be divided into aromatic ring-retaining products (benzaldehyde and phenol), non-aromatic ring-reserved products (furan), and ring-opening carbonyl products (methyl glyoxal, and 2-hydroxy-1,3-propandial). Most of the chemical compositions of SOA particle in our results are the same as those in [2, 5–9]. However, there are some exceptions. This is possibly due to the fact that we detect the particles of SOA using different sample preparation and analyzing technology.

4. Conclusions

A laboratory study was carried out to investigate the secondary organic aerosol products from photooxidation of toluene in a smog chamber. A new laser aerosol time -of-flight mass spectrometer was employed to simultaneously detect the size and composition of the secondary organic aerosol. Some important products such as aldehyde, ketone and carboxylic acid compounds were measured. This will provide new information for discussing toluene–photooxidation reaction mechanism.

Acknowledgements – This work was supported by National Natural Science Foundation of China (20477043) and Knowledge Innovation Foundation of Chinese Academy of Sciences (KJCX2-SW-H08).

References

[1] SONG C., NA K., COCKER D.R., *Impact of the hydrocarbon to NO_x ratio on secondary organic aerosol formation*, Environmental Science and Technology **39**(9), 2005, pp. 3143–9.

[2] JANG M., KAMENS R.M., *Characterization of secondary aerosol from the photooxidation of toluene in the presence of NO_x and 1-propene*, Environmental Science and Technology **35**(18), 2001, pp. 3626–39.

[3] ATKINSON R., *Atmospheric chemistry of VOCs and NO_x*, Atmospheric Environment **34**(12–14), 2000, pp. 2063–101.

[4] SUH I., ZHANG R.Y, MOLINA L.T., MOLINA M.J., *Oxidation mechanism of aromatic peroxy and bicyclic radicals from OH–toluene reactions*, Journal of the American Chemical Society **125**(41), 2003, pp. 12655–65.

[5] FORSTNER H.J.L., FLAGAN R.C., SEINFELD J.H., *Secondary organic aerosol from the photooxidation of aromatic hydrocarbons: molecular composition*, Environmental Science and Technology **31**(5), 1997, pp. 1345–58.

[6] SUH I., ZHANG D., ZHANG R.Y., MOLINA L.T., MOLINA M.J., *Theoretical study of OH addition reaction to toluene*, Chemical Physics Letters **364**(5–6), 2002, pp. 454–62.

[7] SATO K., KLOTZ B., HATAKEYAMA S., IMAMURA T., WASHIZU Y., MATSUMI Y., WASHIDA N., *Secondary organic aerosol formation during the photo-oxidation of toluene: dependence on initial hydrocarbon concentration*, Bulletin of the Chemical Society of Japan **77**(4), 2004, pp. 667–71.

[8] ODUM J.R., HOFFMANN T., BOWMAN F., COLLINS D., FLAGAN R.C., SEINFELD J.H., *Gas/particle partitioning and secondary organic aerosol yields*, Environmental Science and Technology **30**(8), 1996, pp. 2580–5.

[9] STROUD C.A., MAKAR P.A., MICHELANGELI D.V., MOZURKEWICH M., HASTIE D.R., BARBU A., HUMBLE J., *Simulating organic aerosol formation during the photooxidation of toluene/NO_x mixtures: comparing the equilibrium and kinetic assumption*, Environmental Science and Technology **38**(5), 2004, pp. 1471–9.

[10] EDNEY O., DRISCOLL D.J., WEATHERS W.S., KLEINDIENST T.E., CONVER T.S., MCIVER C.D., LI W., *Formation of polyketones in irradiated toluene/propylene/NO_x/air mixtures*, Aerosol Science and Technology **35**(6), 2001, pp. 998–1008.

[11] KLEINDIENST E., CONVER T.S., MCIVER C.D., ENDEY E.O., *Determination of secondary organic aerosol products from the photooxidation of toluene and their implications in ambient $PM_{2.5}$*, Journal of Atmospheric Chemistry **47**(1), 2004, pp. 79–100.

[12] JAOUI M., KLEINDIENST T.E., LEWANDOWSKI M., EDNEY E.O., *Identification and quantification of aerosol polar oxygenated compounds bearing carboxylic or hydroxyl groups. 1. Method development*, Analytical Chemistry **76**(16), 2004, pp. 4765–78.

[13] SUESS D.T.PRATHER K.A., *Mass spectrometry of aerosols*, Chemical Reviews **99**(10), 1999, pp. 3007–35.

[14] PRATHER K.A., NORDMEYER T., SALT K., *Real-time characterization of individual aerosol particles using time-of-flight mass spectrometry*, Analytical Chemistry **66**(9), 1994, pp. 1403–7.

[15] NORDMEYER T., PRATHER K.A., *Real-time measurement capabilities using aerosol time-of-flight mass spectrometry*, Analytical Chemistry **66**(20), 1994, pp. 3540–2.

[16] GARD E., MAYER J.E., MORRICAL B.D., DIENES T., FERGENSON D.P., PRATHER K.A., *Real-time analysis of individual atmospheric aerosol particles: design and performance of a portable ATOFMS*, Analytical Chemistry **69**(20), 1997, pp. 4083–91.

[17] SILVA P.J., PRATHER K.A., *Interpretation of mass spectra from organic compounds in aerosol time-of-flight mass spectrometry*, Analytical Chemistry **72**(15), 2000, pp. 3553–62.

[18] SU Y., SIPIN M.F., FURUTANI H., PRATHER K.A., *Development and characterization of an aerosol time-of-flight mass spectrometer with increased detection efficiency*, Analytical Chemistry **76**(3), 2004, pp. 712–9.

[19] XIA Z.-H., FANG L., ZHENG H.-Y., HU R., ZHANG Y.Y., KONG X.-H., GU X.-J., ZHU Y., ZHANG W.-J., BAO J., XIONG L.-Y., *Real-time measurement of the aerodynamic size of individual aerosol particles*, Acta Physica Sinica **53**(1), 2004, pp. 320–4.

[20] XIA Z.-H., FANG L., ZHENG H.-Y., KONG X.-H., ZHOU L.-Z., GU X.-J., ZHU Y., ZHANG W.-J., *Real-time measurement of chemical compositions of individual aerosol particles*, Chinese Journal of Analytical Chemistry **32**(7), 2004, pp. 973–6.

[21] NIE J.S., QIN M., YANG Y., ZHANG W.-J., *The structure and performance of a kind of photo chemical smog chamber*, Chinese Journal of Atomic and Molecular Physics **19**, 2002, pp. 179–83.

[22] LIU D.Y., WENZEL R.J., PRATHER K.A., *Aerosol time-of-flight mass spectrometry during the Atlanta supersite experiment: 1. Measurements*, Journal of Geophysical Research **108**(D7), 2003, pp. SOS14-1–16.

[23] AYRES R.U., AYRES L.W., *The life-cycle of chlorine, part IV: accounting for persistent cyclic organo-chlorines*, Journal of Industrial Ecology **3**(2–3), 2000, pp. 121–59.

Received October 23, 2005